

Uncovering the identities of compact objects in high-mass X-ray binaries and gamma-ray binaries by astrometric measurements

Masaki S. Yamaguchi,¹★ T. Yano,² and N. Gouda^{2,3}

¹*Institute of Astronomy, Graduate School of Science, University of Tokyo, Mitaka, Tokyo 181-0015, Japan*

²*National Astronomical Observatory, Mitaka, Tokyo 181-8588, Japan*

³*SOKENDAI (The Graduate University for Advanced Students), Shonan Village, Hayama, Kanagawa 240-0193, Japan*

Accepted XXX. Received YYY; in original form ZZZ

ABSTRACT

We develop a method for identifying a compact object in binary systems with astrometric measurements and apply it to some binaries. Compact objects in some high-mass X-ray binaries and gamma-ray binaries are unknown, which is responsible for the fact that emission mechanisms in such systems have not yet confirmed. The accurate estimate of the mass of the compact object allows us to identify the compact object in such systems. Astrometric measurements are expected to enable us to estimate the masses of the compact objects in the binary systems via a determination of a binary orbit. We aim to evaluate the possibility of the identification of the compact objects for some binary systems. We then calculate probabilities that the compact object is correctly identified with astrometric observation (= confidence level) by taking into account a dependence of the orbital shape on orbital parameters and distributions of masses of white dwarfs, neutron stars, and black holes. We find that the astrometric measurements with the precision of $70\mu\text{as}$ for γ Cas allows us to identify the compact object at 99% confidence level if the compact object is a white dwarf with $0.6 M_{\odot}$. In addition, we can identify the compact object with the precision of $10\mu\text{as}$ at 97% or larger confidence level for LS I +61° 303 and 99% or larger for HESS J0632+057. These results imply that the astrometric measurements with the $10\text{-}\mu\text{as}$ precision level can realize the identification of compact objects for γ Cas, LS I +61° 303, and HESS J0632+057.

Key words: astrometry – high-mass X-ray binaries – gamma-ray binaries

1 INTRODUCTION

The binary emitting X-ray is one of the most important targets in high-energy astrophysics. This kind of binary is generally called X-ray binary, which consists of an optical star and a compact object (a neutron star or a black hole). Observations in X-ray bands allowed us to develop the theory of the accretion disk, and many black hole candidates have been discovered from them. Recently, a new binary class called gamma-ray binary, from which gamma rays are observed as well as X-ray (mentioned in detail below), has been discovered (Aharonian et al. 2005). The X-ray emissions from Gamma-ray binaries show power-law spectra, which means that non-thermal electrons (and/or positrons) are accelerated in the binary systems. This implies that the emissions from gamma-ray binaries can provide a clue to the solution of the long-standing problem of the particle accel-

ation. Thus, these binaries become more and more important for the study on high-energy astrophysics.

Emission mechanism has been under discussion for some kinds of binaries, such as γ Cas. The binary γ Cas is one of the peculiar Be/X-ray binaries, which generally consist of a pulsar and a Be star (B star with a circumstellar disk). Although the X-ray source is associated with the Be star, spectral features and X-ray variability of γ Cas are different from those of other typical Be/X-ray binaries. The observational features of γ Cas different from other Be/X-ray binaries are thermal X-ray with high temperature (10–12 keV), relatively low luminosity ($L_x \sim 10^{32-33}$ erg/s), and no flare activity (Lopes de Oliveira et al. 2010, and reference therein). Such peculiar features are observed in some other Be/X-ray binaries, which are called γ Cas like objects (Lopes de Oliveira et al. 2006). Two viable scenarios explaining these X-ray features of γ Cas are proposed; (1) accretion of the matter from the circumstellar disk onto a white dwarf (Lopes de Oliveira et al. 2007) or

★ E-mail: masaki@ioa.s.u-tokyo.ac.jp

a neutron star (White 1982) and (2) magnetic interaction between the stellar surface and the circumstellar disk (e.g., Smith & Robinson 1999). The compact object has not been identified in the former scenario, so that it is unknown that the accretion in the system is similar to that in a cataclysmic variable (a white dwarf) or an X-ray pulsar (a neutron star).

Emission mechanisms in gamma-ray binary systems also have not been understood, mainly because compact objects in most of gamma-ray binaries have never been identified. The gamma-ray binary is a new class of high-mass X-ray binaries (HMXB), which was first discovered in 2004 (Aharonian et al. 2005), and six objects have been identified so far. Non-thermal radio to TeV gamma-ray emissions have been detected from gamma-ray binaries, and some of these emissions vary with the orbital period. However, the emission mechanism has not yet been explained clearly (e.g., Dubus 2013). If the compact object is a neutron star, we expect that the non-thermal emissions are produced at shocks formed by the collision between the pulsar wind and the stellar wind. If it is a black hole instead, we expect that the stellar wind accretes to drive the jet, so that non-thermal emissions can be produced at shocks in the jet (internal shock model) and/or shocks between the jet and the stellar wind (external shock model). Thus, the identification of the compact object allows us to constrain the emission mechanism.

We can identify such unrevealed compact objects by measuring their masses. The masses of white dwarfs, neutron stars, and black holes show different distributions. The mass distribution of the white dwarfs has a peak at 0.5–0.6 M_{\odot} and the masses for almost all of the white dwarfs are below $\sim 1 M_{\odot}$ (Kepler et al. 2016). The masses of the neutron stars distribute between 1.0 and 2.0 M_{\odot} , which are estimated by measuring the mass of neutron stars in neutron star-white dwarf systems and double neutron star systems (Kiziltan et al. 2013). The mass range of black holes is 3–10 M_{\odot} , although their masses have larger uncertainties (Shaposhnikov et al. 2009). Thus, we can statistically identify a compact object by determining the mass of the compact object in a X-ray binary where the compact object has not yet been identified.

Astrometric observations allow us to dynamically measure the mass of such an unseen compact object. The astrometric time-series data of the star with an unseen companion makes it possible to determine all orbital elements, by the use of a method in literature (e.g., Monet 1978; Asada et al. 2004; Asada 2008). Given the mass of the observed star in addition to its orbital elements (especially, the semi-major axis and orbital period), we can estimate the mass of the companion star by using the Kepler’s third law. Thus, it is possible that the astrometric measurements for X-ray binaries and gamma-ray binaries constrain the mass of their compact objects and determine the identity of them (white dwarfs, neutron stars, or black holes). This means that if a compact object in such binaries is unknown, the compact object can be identified by performing the high-precision astrometry.

Recent/future astrometric satellites, such as Gaia and Small-JASMINE, can perform the observation for stellar positions and motions with high precision. The Gaia satellite was launched on 19 December 2013 and its mission period is planned to be around five years. It surveys the whole

sky and observes a billion of stars at G-band (0.3–1.0 μm ; de Bruijne 2012). Gaia measures the positions of photocentres of stellar images with a precision of 7 microarcsecond (μas) for objects brighter than 12 magnitude at G-band, and it observes the same target once per ~ 50 days. Small-JASMINE is planned as the second mission of JASMINE project series (other two missions are called Nano-JASMINE and (medium-sized) JASMINE; Gouda 2011). It will survey the Galactic centre region and observe other some regions including interesting scientific targets at Hw-band (1.1–1.7 μm). Small-JASMINE will perform the astrometric observation with a precision of $\sim 10 \mu\text{as}$ for objects brighter than 12.5 magnitude at Hw-band. Small-JASMINE can observe a certain target once per 100 minutes, which is much more frequent than the observational frequency of Gaia, so that Small-JASMINE can detect short-term variabilities of the photocentres of stellar motions.

The capability of Gaia to detect an unidentified compact companion (neutron star) in HMXBs have been investigated by Maoiléidigh et al. (2005, 2006). The authors calculate the probability distribution function of a semi-major axis of a target OB star which has an unseen companion taking into account the mass transfer and supernova explosion. They then find the probability that the semi-major axis is within the range in which Gaia can detect a neutron star as a companion of OB stars. They obtain the probabilities for some known OB stars as a function of the kick velocity due to the supernova explosion. They also apply their ideas to known HMXBs to obtain the results that an unidentified companion in the γ Cas system can be detected with a probability of 30–50 %, and for the X Per system Gaia can detect a neutron star with a probability of 10–30 %, where the range of these probabilities reflects the range of the kick velocity (0–200 km/s). In addition, by using the semi-major axes for these two systems, which are estimated based on the data of spectroscopic observations, they argue that the companions of these binary systems can be detected by Gaia. We should note that they discuss the possibility that Gaia can detect a compact companion based only on the semi-major axis.

The detectability of an unseen companion with astrometric observations depends not only on the semi-major axis but also the other orbital elements. Asada et al. (2007) have investigated precisions of determining orbital parameters by astrometric observations for elliptical orbits with various values of the eccentricity, inclination angle, and argument of periapsis. They have shown that even if they do not change the semi-major axis, the precision of semi-major axis changes by one order of magnitude. The detection of semi-major axis of the target star means the detection of an unseen companion, so that the precision of semi-major axis can be a criterion of the detection of an unseen companion. Thus, the results of Asada et al. (2007) implies that the eccentricity, inclination angle, and argument of periapsis of the stellar orbit affects the detectability of an unseen companion. Therefore, we should take into account the orbital elements other than the semi-major axis to estimate the possibility that a companion can be detected by astrometric observations.

In this paper, we evaluate possibility that compact objects in specific HMXBs and gamma-ray binaries are correctly identified, which corresponds to a confidence level. To

identify compact objects from their masses, we should incorporate the distributions of white dwarfs, neutron stars, and black holes into a procedure to estimate the astrometric precision. In addition, we take into account these orbital parameters. In this paper, we focus on nearby HMXBs and gamma-ray binaries. We demonstrate the way to calculate confidence levels in Section 2 and show the astrometric precisions required for the identification of unknown compact objects for specific binary systems in Section 3. We then discuss a feasibility of some astrometric missions in Section 4. Finally, we summarize our study in Section 5.

2 METHODS

In this section, we show the method to calculate confidence levels for identifying the compact object in HMXBs and gamma-ray binaries. We derive an expression of a precision of the compact object mass as a function of the compact object mass itself, astrometric precision, and the orbital parameters by using an equation of the error propagation. By giving a probability distribution function and defining the mass boundary between a white dwarf, a neutron star, and a black hole, we show how to calculate a probability that the compact object is correctly identified, which corresponds to the confidence level, for a mass of the compact object and an astrometric precision.

2.1 Precision of the compact object mass

In this subsection, we formulate an expression of a precision of the compact object mass. Before we adopt an equation of the error propagation, we show the relation equation between the compact object mass M_c , stellar mass M_* , orbital period P_{orb} , and semi-major axis of the companion, which is represented as a product of an angular semi-major axis of the companion a_* and distance D :

$$\frac{(M_c + M_*)^2}{M_c^3} = \frac{G}{4\pi^2} \frac{P_{\text{orb}}^2}{(a_* D)^3}, \quad (1)$$

where G is the gravitational constant. This equation means that the identification of compact objects requires measurements of M_* , P_{orb} , a_* , and D with a sufficient accuracy. By using Equation (1) and an equation of the error propagation, we obtain the expression of the precision of the compact object mass σ_m :

$$\left(\frac{\sigma_m}{M_c}\right)^2 = \left(\frac{3}{2} - \frac{M_c}{M_c + M_*}\right)^{-2} \times \left[\left(\frac{M_*}{M_c + M_*}\right)^2 \frac{\sigma_{M_*}^2}{M_*^2} + \frac{\sigma_P^2}{P_{\text{orb}}^2} + \frac{9}{4} \left(\frac{\sigma_a^2}{a_*^2} + \frac{\sigma_D^2}{D^2} \right) \right], \quad (2)$$

where σ_{M_*} , σ_P , σ_a , and σ_D are the standard errors of the companion mass, orbital period, semi-major axis, and distance, respectively. In deriving this equation, we assume that for all variables the ratios of the standard errors to the variables themselves are smaller than 1, and the correlation between errors of these parameters can be neglected. Here, we should note that the correlation between errors of the semi-major axis and distance may be non-negligible if the orbital period is close to 1 year, because the orbital motion is similar to the annual elliptical motion in that case.

We can further reduce Equation (2) by adopting some approximation. Orbital periods of X-ray binaries and gamma-ray binaries is usually well-determined compared to the stellar mass and distance, so that we can neglect the term of the standard error of the orbital period in Equation (2). In addition, the term $\frac{\sigma_D^2}{D^2}$ is expressed as $\frac{\sigma_\pi^2}{\pi_p^2}$, where π_p and σ_π are the parallax and its standard error, respectively, and σ_a can be reduced to be $f(e, i, \omega)\sigma_{\text{mis}}$ (see Appendix A), where $f(e, i, \omega)$ and σ_{mis} are the function of eccentricity e , inclination angle i , and argument of periastris ω (Appendix E, and precisions reachable with a mission, respectively. Thus, Equation (2) can be reduced as

$$\left(\frac{\sigma_m}{M_c}\right)^2 = \left(\frac{3}{2} - \frac{M_c}{M_c + M_*}\right)^{-2} \times \left[\left(\frac{M_*}{M_c + M_*}\right)^2 \frac{\sigma_{M_*}^2}{M_*^2} + \frac{9}{4} \sigma_{\text{mis}}^2 \left(\frac{f^2}{a_*^2} + \frac{1}{\pi_p^2} \right) \right], \quad (3)$$

where we assume that the precision of parallax can be approximated to be that reachable with a mission. We here note that a_* is estimated by using M_c , M_* , P_{orb} , and π_p . Thus, this equation means that we obtain the precision of the compact object mass if we give M_c , σ_{mis} , and parameters inherent to each object (M_* , σ_{M_*} , $f(e, i, \omega)$, P_{orb} , and π_p).

2.2 Confidence level

In this subsection, we demonstrate the way to find confidence levels by calculating the possibility that the compact object is correctly identified. The boundary mass and the probability distribution function of measured mass are required for calculating this possibility. We adopt boundary masses of $1.2 M_\odot$ between a white dwarf and a neutron star and $2.5 M_\odot$ between a neutron star and a black hole (Figure 1). The boundary mass $1.2 M_\odot$ is obtained so that a fraction of white dwarfs below the mass is equal to that of neutron stars above the mass, i.e.,

$$\int_0^{M_{\text{bou}}} F_{\text{WD}}(M) dM = \int_{M_{\text{bou}}}^\infty F_{\text{NS}}(M) dM \sim 0.9, \quad (4)$$

where M_{bou} is the boundary mass between a white dwarf and a neutron star, and F_{WD} and F_{NS} are the probability distribution functions for masses of white dwarfs and neutron stars, respectively. In addition, we should note that F_{NS} has two components; NS-WD system and double NS system. Here, we assume that contributions to all neutron stars of these two components is equal. The last equation of Equation (4) means that tenth of all white dwarfs has a mass larger than $1.2 M_\odot$ and tenth of all neutron stars has a mass smaller than $1.2 M_\odot$. The boundary mass between a neutron star and a black hole, $2.5 M_\odot$, is determined to be a mass where mass distributions of both neutron stars and black holes is nearly zero. This boundary mass is also adopted in [Belczynski et al. \(2008\)](#). We use these boundary masses for judging the identity of the compact object.

We then obtain the confidence level by using probability distribution function of measured mass. Here, we assume that measured mass of a compact object $M_{c,\text{meas}}$ is normally distributed, i.e.,

$$N(M_{c,\text{meas}}; M_c, \sigma_m) \equiv \frac{1}{\sqrt{2\pi}\sigma_m} \exp\left(-\frac{(M_{c,\text{meas}} - M_c)^2}{2\sigma_m^2}\right), \quad (5)$$

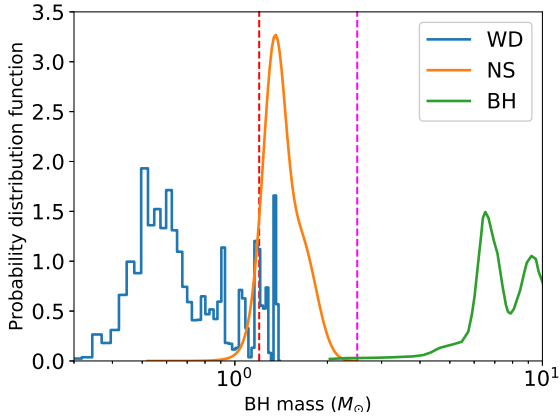


Figure 1. Distributions of masses for white dwarfs, neutron stars, and black holes. We also show the boundary mass between a white dwarf and a neutron star ($1.2M_{\odot}$; red line) and one between a neutron star and a black hole ($2.5M_{\odot}$; magenta line), which are adopted in this paper. The mass distributions of white dwarfs, neutron stars, and black holes are taken from those in Figure 3 of Kepler et al. (2016), Figure 2 of Kiziltan et al. (2013), and Figure 2 of Özel et al. (2010), respectively.

where we note that M_c is a true value of a compact object mass. We further assume that M_c distributes as in Figure 1, so that we find the distribution of measured mass averaged using the distributions of M_c :

$$A_{[\text{WD,NS,BH}]}(M_{c,\text{meas}}; \sigma_{\text{mis}}) \equiv \int N(M_{c,\text{meas}}; M_c, \sigma_m) \times F_{[\text{WD,NS,BH}]}(M_c) dM_c, \quad (6)$$

where F_{BH} is the distribution of black hole mass calculated in Özel et al. (2010), and we note that the function A also different from object to object. In the case that the candidate of the compact object is a white dwarf or a neutron star, the probability that we can correctly identify the compact object $P_{[\text{WD,NS}]}$ can be expressed as follows:

$$P_{\text{WD}}(M_{c,\text{meas}}; \sigma_{\text{mis}}) = \frac{A_{\text{WD}}}{A_{\text{WD}} + A_{\text{NS}}} \text{ for } M_{c,\text{meas}} < 1.2M_{\odot}, \quad (7)$$

$$P_{\text{NS}}(M_{c,\text{meas}}; \sigma_{\text{mis}}) = \frac{A_{\text{NS}}}{A_{\text{WD}} + A_{\text{NS}}} \text{ for } M_{c,\text{meas}} > 1.2M_{\odot}. \quad (8)$$

In the case that the candidate of the compact object is a neutron star or a black hole, the probability that we can correctly identify the compact object $Q_{[\text{NS,BH}]}$ can be expressed as follows:

$$Q_{\text{NS}}(M_{c,\text{meas}}; \sigma_{\text{mis}}) = \frac{A_{\text{NS}}}{A_{\text{NS}} + A_{\text{BH}}} \text{ for } M_{c,\text{meas}} < 2.5M_{\odot}, \quad (9)$$

$$Q_{\text{BH}}(M_{c,\text{meas}}; \sigma_{\text{mis}}) = \frac{A_{\text{BH}}}{A_{\text{NS}} + A_{\text{BH}}} \text{ for } M_{c,\text{meas}} > 2.5M_{\odot}. \quad (10)$$

Thus, if $M_{c,\text{meas}}$ and σ_{mis} are given, we can calculate the confidence level for each binary by using these expressions. Here, we should note that prior probabilities of a white dwarf, a neutron star, and a black hole are identical, because the distributions shown in Figure 1 are all normalised as unity.

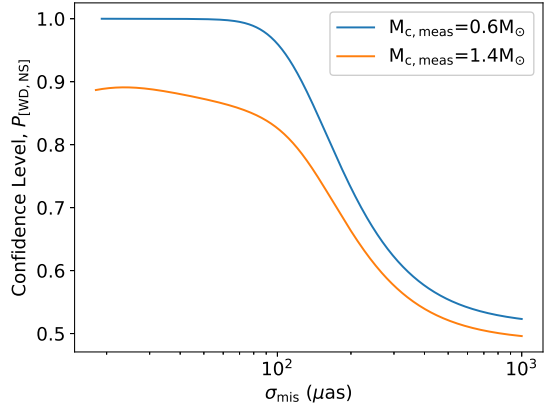


Figure 2. Confidence level as a function of the astrometric precision of a mission for γ Cas. We show the cases that the measured masses of a compact object are $0.6 M_{\odot}$ (blue) and $1.4 M_{\odot}$ (orange).

3 APPLICATION TO A HMXB AND GAMMA-RAY BINARIES

We apply Equations (7-10) to a HMXB and gamma-ray binaries. We search for nearby HMXBs with long orbital periods because they are promising for the detection of the orbit by astrometric observations. Four good candidates are found from the HMXB catalogue (Liu et al. 2006) and listed up in Table 1. Three objects other than γ Cas are known to include a neutron star, so that we focus on γ Cas in Section 3.1. Although five gamma-ray binaries have been detected in Milky Way, the compact objects in the four binaries of them remain unknown (e.g., Dubus 2013), so that we focus on these four gamma-ray binaries in Section 3.2.

3.1 γ Cas (a white dwarf or a neutron star)

A white dwarf or a neutron star is acceptable as the compact object in γ Cas, given the dynamical mass derived with the observation of radial velocity and an assumption of coplanarity between the orbital plane and circumstellar disk (Harmanec et al. 2000). We calculate the precisions of $f(e, i, \omega)$ for γ Cas in the way stated in Appendix D. The eccentricity and argument of periapsis of γ Cas are measured as 0.26 and $\sim 50^\circ$, respectively, from the observation of H α emission (Harmanec et al. 2000), so that $f(e, i, \omega)$ of γ Cas is calculated as 1.4. Here, we note that $f(e, i, \omega)$ is nearly independent of the inclination angle when the argument of periapsis ω is small, which is shown in the second paragraph of Appendix F. In addition, as shown in Table 1, the mass of companion star in the γ Cas system, the parallax, and the orbital period are $19 \pm 0.1M_{\odot}$, 5.9 mas, and 204 days, respectively.

We obtain the relations between confidence levels and σ_{mis} for given measured masses, which are shown in Figure 2. Here, we assume that the measured masses are $0.6 M_{\odot}$ (a white dwarf is assumed and Equation 7 is used) and $1.4 M_{\odot}$ (a neutron star is assumed and Equation 8 is used). For a white dwarf case, the confidence level reaches ≈ 1.0 below $\sim 70 \mu\text{as}$, while it is below 0.9 at a maximum for a neutron star case. This is because the distribution of white

Table 1. A high-mass X-ray binaries selected from the catalogue, “Catalogue of Galactic high-mass X-ray binaries” (Liu et al. 2006) and five gamma-ray binaries.

Object name	V (mag)	H (mag)	M_* (M_\odot)	Parallax (mas)	Distance (kpc)	P (days)	$f(e, i, \omega)$	Pulsar?
γ Cas	1.6 ^a	2.0 ^a	19 \pm 0.1 ^b	5.9 ^c		204 ^a	1.4	unknown
X Per	6.0 ^a	6.1 ^a	15 \pm 0.8 ^b	2.3 ^c		250 ^a	1.4	yes
V725 Tau	8.9 ^a	8.3 ^a	8 \pm 0.3 ^b	3.7 ^c		111 ^a	1.4	yes
V801 Cen	9.3 ^a	8.6 ^a	9 \pm 0.4 ^b	1.8 ^c		188 ^a	>1.4	yes
LS 5039	11.2	8.8 ^d	23 \pm 3 ^e		2.5 ^f	3.9 ^f	1.4	unknown
1FGL J1018.6-5856	12.9	10.1 ^d	\sim 37 ^e		5 ^f	16 ^f	(1.4)	unknown
LS I +61° 303	10.8	8.2 ^d	12.5 \pm 2.5 ^e		1.9 ^f	26 ^f	1.3	unknown
HESS J0632+057	9.1	7.4 ^d	16 \pm 3 ^e		1.4 ^f	320 ^f	3.8-5.4	unknown
PSR B1259-63	9.3	8.6 ^d	31 ^e		2.3 ^f	1237 ^f	3.6-3.7	yes

The former four objects are categorized as high-mass X-ray binaries, and the others are gamma-ray binaries.

^a Appeared in the HMXB catalogue (Liu et al. 2006). ^b Appeared in the catalogue “A catalog of young runaway *Hipparcos* stars within 3 kpc from the Sun” (Tetzlaff et al. 2011). ^c Values appeared in *Hipparcos* catalogue (van Leeuwen 2007). ^d 2MASS All-Sky Catalog of Point Sources (Skrutskie et al. 2006). ^e We adopt the middle values of the mass ranges appeared in Casares et al. (2012). ^f Values appeared in Casares et al. (2012).

dwarf mass (Figure 1) extends to $\sim 1.4 M_\odot$, while that of neutron star mass shows nearly zero at $1.0 M_\odot$. Even if the astrometric precision is high enough, a white dwarf with $\sim 1.4 M_\odot$ is expected to exist, so that the probability that the compact object with a mass of $1.4 M_\odot$ is a white dwarf is non-zero. The minimum values for σ_{mis} is determined by the corresponding σ_m of $0.05 M_\odot$, because the intervals of bins in the distribution of white dwarf mass is ~ 0.03 , which means that the integration of Equation (6) is affected by one normal distribution corresponding to one bin if $\sigma_m \lesssim 0.03$.

Based on Figure 2, we argue that $\sigma_{\text{mis}} \sim 70 \mu\text{as}$ is enough to identify the compact object in γ Cas if the compact object has the typical mass of a white dwarf or a neutron star. With such σ_{mis} , we can identify a white dwarf with a typical mass ($0.5\text{--}0.6 M_\odot$) at $\sim 99\%$ confidence level, where we can expect that in the case of a white dwarf with $0.5 M_\odot$, the confidence level gets higher than that with $0.6 M_\odot$, because $0.5 M_\odot$ is farther from the mass distribution of neutron stars. In addition, we can identify a neutron star with a typical mass ($\sim 1.4 M_\odot$) with $\sim 90\%$ confidence level.

3.2 Gamma-ray binaries (a neutron star or a black hole)

Applying Equations (9 and 10) to gamma-ray binaries allows us to obtain confidence levels for determining whether the compact object is a neutron star or a black hole. In Table 1, we show the V and H magnitudes, the stellar masses, the distances from the Earth, the orbital periods, and the functions $f(e, i, \omega)$ for five galactic gamma-ray binaries. Here, the error of stellar mass for 1FGL J1018.6-5856 is not shown, so that we adopt $\sigma_{M_*} = 5 M_\odot$. This is just an assumption, but the results do not change if σ_{M_*} is less than the stellar mass itself, because the dominant term in the right-hand side of Equation (3) is the term of σ_{mis} for 1FGL J1018.6-5856.

The functions $f(e, i, \omega)$ are calculated by using known values of e and ω . We adopt $e = 0.24$ and $\omega = 237^\circ$ for LS 5039 (Sarty et al. 2011), $e = 0.54$ and $\omega = 41^\circ$ for LS I +61° 303 (Aragona et al. 2009), $e = 0.83$ and $\omega = 129^\circ$ for HESS J0632+057 (Casares et al. 2012), and $e = 0.87$ and $\omega = 139^\circ$ for PSR B1259-63 (Johnston et al. 1994). For the inclination angle in the function f , we adopt 10° and 80° be-

cause of its uncertainty in the radial velocity measurements. If the eccentricity is large and the argument of periapsis is close to 90° , the uncertainty of the inclination angle affects the $f(e, i, \omega)$ values (Appendix F). Thus, the $f(e, i, \omega)$ values of HESS J0632+057 and PSR B1259-63 are affected by the uncertainty of i , so that Table 1 shows the ranges of the $f(e, i, \omega)$ values for HESS J0632+057 and PSR B1259-63. Here, we should note that the f values reach 4 or 5 for the high eccentric systems (HESS J0632+057 and PSR B1259-63), which means that if we neglect this factor, we overestimate the required astrometric precision by a factor of 4 or 5 for high eccentric systems. The orbital elements of 1FGL J1018.6-5856 have not yet determined, so that we assume the typical value, 1.4. Here, we adopt a middle value, 4.6, as f of HESS J0632+057.

We show the confidence levels for four gamma-ray binaries in Figure 3, adopting the measured mass of $1.4, 5.0$, and $10 M_\odot$, where we assume that the compact object masses of 5.0 and $10 M_\odot$ are less and more massive black holes, respectively. Confidence levels of all binaries at the minimum σ_{mis} reach 1.0, which is because the distributions of neutron star mass and black hole mass show little overlap (Figure 1), so that we can certainly identify the compact object for small σ_{mis} , that is, small σ_m . Figure 3 also shows that the confidence levels of the measured mass $5.0 M_\odot$ is higher than those of $10 M_\odot$. This is due to the difference between the measured mass and the mass range of the neutron star. When the measured mass is farther from the mass range of neutron star, A_{NS} is smaller compared to A_{BH} , so that the confidence level is higher.

In addition, we see for all binaries that the confidence level of $M_{\text{c, meas}} = 1.4 M_\odot$ at the maximum σ_{mis} is larger than 0.5, while that of $M_{\text{c, meas}} = 5.0$ and $10 M_\odot$ is smaller than 0.5. This is due to the distributions of neutron star mass and black hole mass. For a large σ_m , the distribution of measured mass can be approximated to be $(2\pi)^{-1/2} \sigma_m^{-1}$ (see Equation 5), so that Q_{NS} and Q_{BH} are proportional to $\langle \sigma_m^{-1} \rangle_{\text{NS}}$ and $\langle \sigma_m^{-1} \rangle_{\text{BH}}$, respectively, where $\langle x \rangle_{[\text{NS, BH}]}$ means the statistical average of x for the distribution of neutron star mass or black hole mass. We can derive $\sigma_m \sim M_{\text{c}} \sigma_{\text{mis}} / a_*$ from Equation (3) for the current situation (large σ_{mis} , $a_* < \pi_p$, and $M_{\text{c}} < M_*$), so that by using Equation (1), $\sigma_m \propto (M_{\text{c}} +$

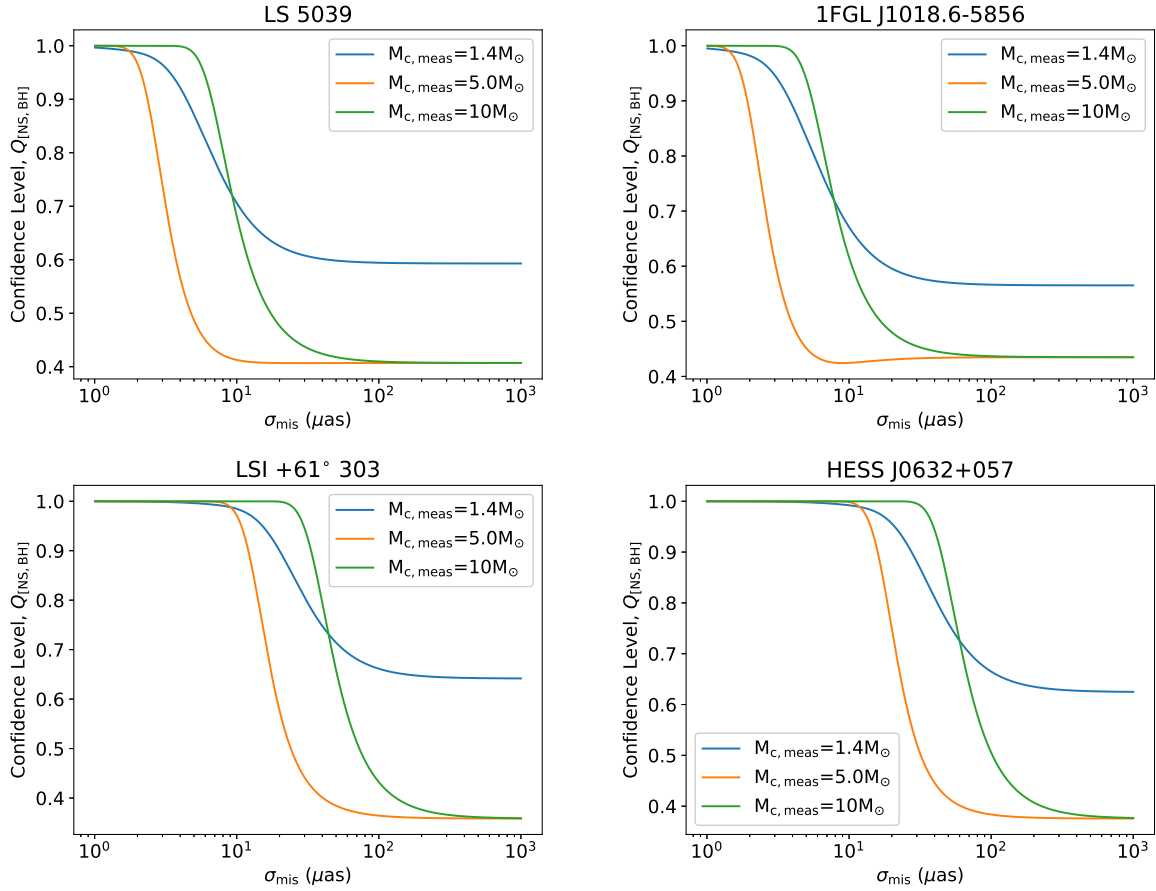


Figure 3. Same as Figure 2 for gamma-ray binaries. We adopt the measured masses of 1.4, 5.0, and 10 M_{\odot} .

$M_*)^{2/3}$. This means that the larger M_c leads to the larger σ_m . Therefore, Q_{NS} is larger than Q_{BH} at a large σ_{mis} . This implies that if σ_{mis} is large, a neutron star is tend to be chosen as a compact object, even if the compact object is a black hole.

For LS 5039 and 1FGL J1018.6-5856, the astrometric precision of 2 μas is required for identifying the compact object at high confidence level ($> 90\%$). The confidence levels of these two binaries (upper panels in Figure 3) are quite similar with each other, because the values of a_* , which is a parameter related to the orbital size on the celestial sphere, for two binaries are nearly identical. When we adopt 90% as a required confidence level, the corresponding values of σ_{mis} are $\sim 2 \mu\text{as}$, $\sim 4 \mu\text{as}$, and $\sim 6 \mu\text{as}$ for $M_{c, meas} = 5.0, 1.4$, and $10 M_*$, respectively. If we allow the confidence level to be 70%, we can identify the compact object with $\sigma_{mis} = 10 \mu\text{as}$ for $M_{c, meas} = 1.4$ and $10 M_{\odot}$.

For LS I +61° 303 and HESS J0632+057, the astrometric precision of 10 μas is enough for identifying the compact object. When we adopt the 90% confidence level, $\sigma_{mis} = 12, 20$, and, $33 \mu\text{as}$ are required for identifying the compact object whose measured masses are 5.0, 1.4, and 10 M_{\odot} , respectively, for LS I +61° 303. For HESS J0632+057, the required astrometric precisions are 16, 28, and 44 μas for the measured masses, 5.0, 1.4, and 10 M_{\odot} , respectively. In addition, when we adopt an astrometric precision of 10 μas ,

the confidence levels for the measured mass of 1.4, 5.0, and 10 M_{\odot} are 97% or larger for LS I +61° 303 and 99% or larger for HESS J0632+057. These results implies that with 10- μas astrometric precision, we can identify the compact object in LS I +61° 303 and HESS J0632+057 at $>97\%$ confidence level if the measured mass is $\sim 1.4 M_{\odot}$ or $> 5.0 M_{\odot}$.

4 FEASIBILITY OF THE SCIENCE OBJECTIVES FOR THE FUTURE/ON-GOING ASTROMETRIC MISSIONS

In this subsection, we discuss the feasibility of the science objectives stated in Sections 3 by the future/on-going astrometric missions, Gaia, Small-JASMINE, GRAVITY of VLTI, and TMT. All these missions aim to achieve the 10- μas level precision. If the precision of 10 μas is achieved for the observation of binaries listed in this paper, we will accomplish the identification of the compact object through the determination of the compact object mass for γ Cas, LS I +61° 303 and HESS J0632+057 at $\sim 90\%$ or larger confidence level, and for LS 5039 and 1FGL J1018.6-5856 at 70% confidence level.

The ground-based telescopes, TMT and GRAVITY, have a critical issue in terms of reference stars for observing these objects. The instrument IRIS imager will be

used for astrometric observations with TMT. To realise the 10- μ as level astrometry with the IRIS imager, some reference stars are required in a field of view of each target object (Schöck et al. 2014). The field of view of the IRIS imager is 17" x 17", so that it is necessary that some reference stars are located within $\sim 10''$ from each target. However, no source is found within 20" from γ Cas, HESS J0632+057, and X Per according to the 2MASS catalogue (Skrutskie et al. 2006). In addition, although one source 5" away from V725 Tau is listed in the 2MASS catalogue (Skrutskie et al. 2006), it is based on low quality results, and no other source is found within 20". Therefore, the identification of the compact object for binaries listed in this paper is not possible with TMT/IRIS. The field of view of VLTI/GRAVITY is 2" for unit telescopes or 4" for auxiliary telescopes (Eisenhauer et al. 2011), so that it is thought to be impossible to realize the identification of the compact object.

The space telescopes for the astrometric observation, Gaia and Small-JASMINE, are promising for the identification of the compact object. The fields of view of these satellites are the order of 1 square degree, where reference stars are included enough to calibrate the stellar position. Besides the field of view, to achieve these science objectives, the observational period longer than orbital periods of the binaries and ten-time or more visits to the binaries are required for measuring the position of whole orbits. The Gaia satellite will visit to all sources on average 70 times for the five-year observation (de Bruijne 2012), and for Small-JASMINE, whose observational period is 3 years, we can adjust the number of visits for individual source (Gouda 2011). Therefore, these satellites will perform the 10- μ as level astrometry without any problems in terms of not only reference stars but also the observational period and the visit number.

5 CONCLUSIONS

We have estimated in this paper probabilities that compact object in γ Cas and four gamma-ray binaries are correctly identified (= confidence levels) as a function of a compact object mass measured by astrometric observation of the binary orbits and an astrometric precision. In the procedure to estimate the confidence levels, we have incorporated the effect of the orbital elements (eccentricity, inclination angle, and argument of periastron) on the precision of semi-major axis and the distributions of masses of white dwarfs, neutron stars, and black holes, which are based on observations. The former effect appears in the relation equation between the precision of semi-major axis and the astrometric precision (the function f in Equation A4), and the resultant astrometric precision is up to 5 times larger than that without this effect. The later one is needed as a prior distribution of compact object masses. We obtain three results as follows by applying this procedure to HMXBs and gamma-ray binaries.

(1) γ Cas is one of the nearest X-ray binaries and whether the compact object in this system is a white dwarf or a neutron star remains unclear (e.g., Lopes de Oliveira et al. 2010). We have found that the astrometric measurements with the precision of 70 μ as allows

us to identify the compact object as a white dwarf at 99% confidence level if the measured mass is 0.6 M_{\odot} . With such astrometric precision, we can identify the compact object as a neutron star at 85% confidence level if the measured mass is 1.4 M_{\odot} .

(2) Compact objects of four gamma-ray binaries, LS 5039, 1FGL J1018.6-5856, LS I +61° 303, and HESS J0632+057, remains unknown. For the former two systems, LS 5039 and 1FGL J1018.6-5856, the precision of 2 μ as is required for identifying the compact object as a black hole at 90% confidence level if the measured mass is 5.0 M_{\odot} . If the measured mass is 1.4 or 10 M_{\odot} , we can identify the compact object with ~ 10 - μ as level astrometry at 70% confidence level.

(3) For latter two systems, LS I +61° 303 and HESS J0632+057, the precision of 10- μ as level is enough for judging their compact objects. In the case of such astrometric precision, the confidence levels for the measured mass of 1.4, 5.0, and 10 M_{\odot} are 97% or larger for LS I +61° 303 and 99% or larger for HESS J0632+057.

The optical astrometric satellite, Gaia, is now operated by European Space Agency, and in the future, Small-JASMINE planned in Japanese group will also perform astrometric measurements. These missions aim to achieve the astrometric precision of the 10- μ as level. Therefore, these missions could contribute the realization of these science objectives.

ACKNOWLEDGEMENTS

We are grateful to H. Asada, K. Yamada, and T. Hara for useful discussions and T. Mihara for useful comments. This work was supported by the JSPS KAKENHI Grant Number JP23244034 and JP15H02075 (both are Grant-in Aid for Scientific Research (A)).

REFERENCES

- Aharonian, F., Akhperjanian, A. G., Aye, K.-M., et al. 2005, *A&A*, 442, 1
- Aitken, R. G. 1964, *The Binary Stars* (New York: Dover)
- Aragona, C., McSwain, M. V., Grundstrom, E. D et al. 2009, *ApJ*, 698, 514
- Asada, H., Akasaka, T., & Kasai, M. 2004, *PASJ*, 56, L35
- Asada, H., Akasaka, T., & Kudoh, M. 2007, *AJ*, 133, 1243
- Asada, H. 2008, *PASJ*, 60, 843
- Belczynski, K., Kalogera, V., Rasio, F. A. et al. 2008, *ApJS*, 174, 223
- Casares, J., Ribó, M., Ribas, I., Paredes, J. M., Vilardell, F. & Negueruela, I. 2012, *MNRAS*, 421, 1103
- de Bruijne, J. H. J. 2012, *ApSS*, 341, 31
- Delgado-Martí, H., Levine, A. M., Pfahl, E., & Rappaport, S. A. 2001, *ApJ*, 546, 455
- Demorest, P. B., Pennucci, T., Ransom, S. M., Roberts, M. S. E., & Hessels, J. W. T. 2010, *Nature*, 467, 1081
- Dubus, G. 2013, *A&ARv*, 21, 64
- Eisenhauer, F., Perrin, G., Brandner, W., et al. 2013, *Messenger*, 143, 1
- Finger, M. H., Wilson, R. B., & Harmon, B. A. 1996, *ApJ*, 459, 288
- Gouda, N. 2011, *Scholarpedia*, 6 (10):12021, <http://www.scholarpedia.org/article/JASMINE>
- Harmanec, P., Habuda, P., Štefl, S., et al. 2000, *A&A*, 364, L85

- Henry, G. W. & Smith, M. A. 2012, *ApJ*, 760, 10
- Iwama, H., Asada, H., & Yamada, K. 2013, *PASJ*, 65, 2
- Johnston, S., Manchester, R. N., Lyne, A. G. et al. 1994, *MNRAS*, 268, 430
- Kepler, S. O., Pelisoli, I., Koester, D. et al. 2016, *MNRAS*, 455, 3413
- Kiziltan, B., Kottas, A., De Yoreo, M., & Thorsett, S. E. 2013, *ApJ*, 778, 66
- Liu, Q. Z., van Paradijs, J., & van den Heuvel, E. P. J. 2006, *A&A*, 455, 1165
- Lopes de Oliveira, R., Motch, C., Haberl, F., Negueruela, I., & Janot-Pacheco, E. 2006, *A&A*, 454, 265
- Lopes de Oliveira, R., Motch, C., Smith, M. A., Negueruela, I., & Torrejón, M. 2007, *A&A*, 474, 983
- Lopes de Oliveira, R., Smith, M. A., & Motch, C. 2010, *A&A*, 512, 22
- Monet, D. G. 1978, *ApJ*, 223, L101
- Maoiléidigh, C. Ó, Meurs, E. J. A., & Norci, L. 2005, *New Astronomy*, 10, 591
- Maoiléidigh, C. Ó, Meurs, E. J. A., & Norci, L. 2006, *Proc. IAU Symp.*, 230, 43
- Özel, F., Psaltis, D., Narayan, R. & McClintock, J. E. 2010, *ApJ*, 725, 1918
- Raguzova, N. V., & Lipunov, V. M. 1998, *A&A*, 340, 85
- Samus, N. N., Durelevich, O. V. et al. 2009, *yCat*, 102025
- Sarty, G. E., Szalai, T., Kiss, L. L. et al. 2011, *MNRAS*, 411, 1293
- Schöck, M., Do, T., Ellerbroek, B. L., et al. 2014, *Proc. SPIE*, 9148, 91482L
- Shaposhnikov, N., & Titarchuk, L. 2009, *ApJ*, 699, 453
- The Two Micron All Sky Survey (2MASS) Skrutskie, M. F., Cutri, R. M., Stiening, M. D. et al. 2006, *AJ*, 131, 1163
- Smith, M. A., & Robinson, R. D. 1999, *ApJ*, 517, 866
- Steele, I. A., Negueruela, I., Coe, M. J., & Roche, P. 1998, *MNRAS*, 297, L5
- Telting, J. H., Waters, L. B. F. M., Roche, P. et al. 1998, *MNRAS*, 296, 785
- Tetzlaff, N., Neuhäuser, R., & Hohle, M. M. 2011, *MNRAS*, 410, 190
- van Leeuwen, F. 2007, *A&A*, 474, 653
- Watson, M. G., Warwick, R. S., & Ricketts, M. J. 1981, *MNRAS*, 195, 197
- White, N. E., Swank, J. H., Holt, S. S., & Parmar, A. 1982, *ApJ*, 263, 277
- Yamada, K., Yamaguchi, M. S., Asada, H., & Gouda, N. 2014, *PASJ*, 66, 97

APPENDIX A: PRECISION OF THE SEMI-MAJOR AXIS

Here, we derive the precision of the semi-major axis, σ_a , by giving a certain set of orbital elements $\vec{\theta} \equiv (a, e, i, \omega, \Omega)$, where a, e, i, ω , and Ω are the semi-major axis, eccentricity, inclination angle, argument of periapsis, and longitude of the ascending node, respectively. Here, we note that the orbital period P is not listed in $\vec{\theta}$. This is because orbital periods of systems focused in this paper (nearby HMXBs and gamma-ray binaries) have been measured with small (typically less than a few percent) uncertainties, so that, in this paper, we assume that the orbital period is a known element. In what follows, we identify the precision of each orbital element with the standard deviation σ_k ($k = 1, 2, 3, 4, 5$), where the integer $k = 1$ corresponds to a , 2 to e , 3 to i , 4 to ω , and 5 to Ω . The dispersion of each orbital element σ_k^2 can be represented by using each diagonal component of a variance matrix V , i.e.,

$$\sigma_k^2 = (V)_{kk}, \quad (\text{A1})$$

The variance matrix V in Equation (A1) can be obtained by calculating variances for estimated values of orbital elements $\vec{\theta}$, so that it depends on methods for the estimation.

If we adopt the least-square method as an estimation method in deriving the orbital elements, then we obtain

$$V = (D^T D)^{-1} \sigma^2, \quad (\text{A2})$$

where σ^2 is a dispersion of the positional data and a matrix D represents a design matrix, whose components are the derivatives of the elliptical orbit on the celestial plane with respect to the orbital elements (see Appendix C). Here, we note that the components of D are two-dimensional vectors and that the multiplication between a component of D^T and one of D in Equation (A2) is an inner product. The reason why we use the least-square method is that we can use the information of both spatial and time with this method and that the expression of the dispersion (Equation A2) is simple enough for us to analytically obtain precisions of orbital elements. On the other hand, in the moment approach, which is another way to estimate the orbital elements and developed by Iwama et al. (2013); Yamada et al. (2014), the timing information is not basically taken into account, so that we obtain the resultant orbital elements with relatively large uncertainties. Thus, this approach will be used to find the trial values of the parameters at the initial stage of an iteration process in the least-square method. Here, we note that the equation of the orbit is a non-linear equation, so that we need to make use of the steepest descent method or Gauss-Newton method, which include the iteration process, to find a set of estimated values of orbital elements.

Thus, the relation between the astrometric precision σ and the precision of the semi-major axis is represented as

$$\sigma_1^2 = (D^T D)_{11}^{-1} \sigma^2, \quad (\text{A3})$$

where the subscription, 11, represents the (1,1) component of the matrix. A point to notice is that the set of the estimated orbital elements $\vec{\theta}$, which is an argument of the matrix D , will be obtained only after we analyse actual observational data. Therefore, in Section 3 we adopt known orbital elements obtained by observations of radial velocities for some specific binaries.

We can further reduce Equation (A3) to obtain the expression (see Appendix E):

$$\sigma_a = f(e, i, \omega) \frac{\sigma}{\sqrt{N}}, \quad (\text{A4})$$

where the precision σ_1 is replaced to σ_a and N is the number of the positional data for the optical star. The coefficient f in Equation (A4) is a function of the orbital elements e, i , and ω (Appendix E) and accurately calculated by a procedure in Appendix D.

APPENDIX B: ELLIPTICAL ORBIT ON THE CELESTIAL SPHERE

In this section we formulate the elliptical motion on the celestial sphere. First, we present an elliptical orbit of a target star in a binary projected on the sky plane (the tangential plane of the celestial sphere at the target star) \vec{r} ;

$$\vec{r} = T \vec{r}_{\text{ell}}, \quad (\text{B1})$$

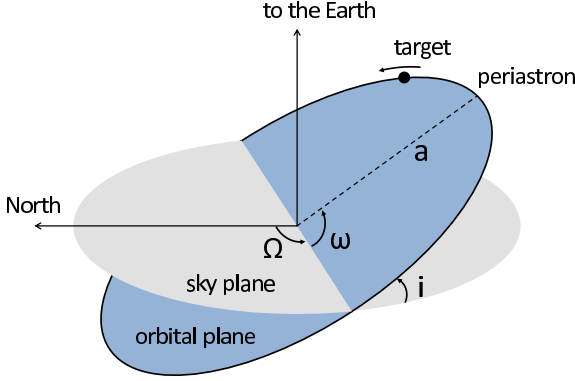


Figure A1. Sketch of an elliptical orbit of a target star in a binary. The gray and blue surfaces are the sky plane and the orbital plane, respectively. The semi-major axis is shown with a dashed line whose length is a , and its direction on the orbital plane is characterized by the argument of periapsis ω . The normal direction to the orbital plane is characterized by the inclination angle i and the longitude of ascending node Ω . The direction “North” represents the direction to the celestial north pole.

where T is the matrix whose components are Thiele-Innes elements (e.g., Aitken 1964);

$$T = \begin{pmatrix} A & F \\ B & G \end{pmatrix} \quad (\text{B2})$$

$$A = a(\cos \omega \cos \Omega - \mu \sin \omega \sin \Omega) \quad (\text{B3})$$

$$B = a(\cos \omega \sin \Omega + \mu \sin \omega \cos \Omega) \quad (\text{B4})$$

$$F = a(-\sin \omega \cos \Omega - \mu \cos \omega \sin \Omega) \quad (\text{B5})$$

$$G = a(-\sin \omega \sin \Omega + \mu \cos \omega \cos \Omega). \quad (\text{B6})$$

Here a, μ, ω, Ω are the angular distance of the semi-major axis, the cosine of the inclination angle i , the argument of periapsis and the longitude of ascending node, respectively (Figure A1). The vector \vec{r}_{ell} in Equation (B1) represents the elliptical orbit on the orbital plane whose semi-major axis is normalised as unity and whose focal point is at the origin, that is,

$$\vec{r}_{\text{ell}} = \begin{pmatrix} \cos E - e \\ \sqrt{1 - e^2} \sin E \end{pmatrix}, \quad (\text{B7})$$

where E and e is the eccentric anomaly and the eccentricity, respectively. Note that in Equation (B1) we assume that we can take the frame moving with the helical motion which consists of the proper motion and the elliptical annual motion of the target star. This assumption is valid if the observational period is larger than one year, if the orbital period of the binary is comparable to or shorter than the observational period, and if the orbital shape or phase of the binary is different from that of the annual elliptical motion. Under these two conditions, the proper motion and parallax are measured separately from the orbital motion. Moreover, we note that the binary orbit is determined if five orbital elements, a, e, i, ω, Ω is fixed.

Given observational data, the orbital equation (Equation B1) includes two more elements. The time t is related to the eccentric anomaly E through the mean anomaly M

as follows,

$$M = 2\pi \frac{t - t_0}{P} = E - e \sin E, \quad (\text{B8})$$

where t_0 and P is the time of periastron passage and the orbital period, respectively. Here, we assume that t_0 and P are obtained by the observation of radial velocity due to the orbital motion, but in this paper we pick up only the binaries whose two elements, t_0 and P , have been already measured. Thus, E is uniquely determined if the observational time is given.

APPENDIX C: DESIGN MATRIX FOR THE LEAST SQUARE METHOD

Here, we linearize Equation (B1) to apply the least-square method to estimation of the orbital elements and their dispersions. Hereafter, we express the orbital elements as a column vector, $\vec{\theta} \equiv (a \ e \ \mu \ \omega \ \Omega)^T$, where the superscript T represents transposition. We will obtain positions of a target star on the celestial sphere at many times provided by Small-JASMINE and Gaia. We define N as the number of the positional data, \vec{X}_j as the j -th positional data which do not include the proper motion and the annual elliptical motion, and E_j as the j -th eccentric anomaly corresponding to the time of the j -th positional data. Thus, we can express \vec{X}_j as

$$\vec{X}_j = \vec{r}(E_j; \vec{\theta}) + \vec{\epsilon}_j \quad (j = 1, \dots, N), \quad (\text{C1})$$

where $\vec{\epsilon}_j$ represents a residual vector of the j -th observational data. By expanding $\vec{r}(E_j; \vec{\theta})$ around a set of trial orbital elements $\vec{\theta}_0$, we find

$$\vec{X}_j = \vec{r}(E_j; \vec{\theta}_0) + D_j \cdot d\vec{\theta} + \vec{\epsilon}_j \quad (j = 1, \dots, N), \quad (\text{C2})$$

where

$$D_j = \left. \frac{\partial \vec{r}(E_j; \vec{\theta})}{\partial \vec{\theta}} \right|_{\vec{\theta}=\vec{\theta}_0}, \quad (\text{C3})$$

and $d\vec{\theta}$ represents a column vector of differentials for the orbital elements. We define a differential position $d\vec{X}_j \equiv \vec{X}_j - \vec{r}(E_j; \vec{\theta}_0)$ and gather N equations of the positional data together, so that we obtain

$$dX = D d\vec{\theta} + \epsilon, \quad (\text{C4})$$

where

$$dX \equiv (d\vec{X}_1 \ \dots \ d\vec{X}_N)^T \quad (\text{C5})$$

$$D \equiv \begin{pmatrix} \frac{\partial \vec{r}_1}{\partial a} & \frac{\partial \vec{r}_1}{\partial e} & \frac{\partial \vec{r}_1}{\partial \mu} & \frac{\partial \vec{r}_1}{\partial \omega} & \frac{\partial \vec{r}_1}{\partial \Omega} \\ \vdots & \vdots & \vdots & \vdots & \vdots \\ \frac{\partial \vec{r}_N}{\partial a} & \frac{\partial \vec{r}_N}{\partial e} & \frac{\partial \vec{r}_N}{\partial \mu} & \frac{\partial \vec{r}_N}{\partial \omega} & \frac{\partial \vec{r}_N}{\partial \Omega} \end{pmatrix} \quad (\text{C6})$$

$$\epsilon \equiv (\vec{\epsilon}_1 \ \dots \ \vec{\epsilon}_N)^T, \quad (\text{C7})$$

where \vec{r}_j ($j = 1, \dots, N$) in the matrix D represent $\vec{r}(E_j; \vec{\theta})$. We note that the $N \times 5$ matrix D , which is called a design matrix, depends on $\vec{\theta}_0$ and that its components are two-dimensional vectors. We adopt $d\vec{\theta}$ at which the norm of ϵ reaches a minimum as the estimated value. If we assign the

value $\vec{\theta}_0 + d\vec{\theta}$ to $\vec{\theta}_0$ in Equation (C4) to find a new $d\vec{\theta}$ at which the norm of ϵ reaches a minimum, then we obtain better solution for the orbital elements. By iterating this procedure until $d\vec{\theta}$ converges at 0, we find the estimated value of $\vec{\theta}$. In the actual analysis, we will stop the iteration when $|d\vec{\theta}|/|\vec{\theta}_0|$ is sufficiently smaller than unity, e.g., 0.01.

APPENDIX D: CALCULATIONAL PROCEDURE OF PRECISIONS OF ORBITAL ELEMENTS

Here, we describe how to compute the precisions σ_k (Equation A1), taking into account the actual observation. In Equation (A2), we have shown that the precisions of orbital elements are represented using $D^T D$, where the expression of the matrix D is represented in Appendix C. Thus, we should reduce $D^T D$ to obtain the precisions.

We first assume that all time intervals between two consecutive data are equal, so that we can replace approximately the summation in the components of the 5×5 matrix $D^T D$ with integration with respect to time. We can express an lm component of the matrix $D^T D$ as

$$(D^T D)_{lm} = \sum_{j=1}^N \frac{\partial \vec{r}_j}{\partial \theta_l} \cdot \frac{\partial \vec{r}_j}{\partial \theta_m} = \frac{N}{P} \int_{t_0}^{t_0+P} \frac{\partial \vec{r}(E)}{\partial \theta_l} \cdot \frac{\partial \vec{r}(E)}{\partial \theta_m} dt, \quad (\text{D1})$$

where we note that the eccentric anomaly E is a single-valued function of the time t . Equation (D1) is valid when the orbital period is shorter than the observational period, i.e., the time it takes to obtain N positional data. For example, Gaia observes an identical object by ~ 80 times for 5 years (de Bruijne 2012), so that we can apply it to binaries with $P < 5$ yrs.

Equation (D1) is further reduced by a variable transformation,

$$dt = \frac{dt}{dE} dE = \frac{P}{2\pi} (1 - e \cos E) dE. \quad (\text{D2})$$

Using this relation, we obtain the expression,

$$(D^T D)_{lm} = \frac{N}{2\pi} \int_0^{2\pi} \frac{\partial \vec{r}(E)}{\partial \theta_l} \cdot \frac{\partial \vec{r}(E)}{\partial \theta_m} (1 - e \cos E) dE. \quad (\text{D3})$$

Since the integrand in Equation (D3) is represented with a quadratic of sine and cosine, the integration is readily performed. Thus, we obtain the precisions of orbital elements by computing the inverse matrix of $D^T D$ using Equation (D3).

APPENDIX E: ORDER ESTIMATION OF THE PRECISIONS

Here, we estimate the orders of σ_k ($k = 1, \dots, 5$) before the accurate calculations. The order of $|\partial \vec{r} / \partial \theta_1|$ are 1 because it is rewritten as $|\vec{r}|/a$, while the orders of $|\partial \vec{r} / \partial \theta_k|$ ($k = 2, 3, 4, 5$) are a . Thus, from Equation (D3) the orders of $(D^T D)_{lm}$ are

as follows.

$$(D^T D)_{lm} = \begin{cases} O(1)N & \text{for } l = m = 1 \\ O(1)aN & \text{for } l = 1 \text{ or } m = 1 \\ O(1)a^2N & \text{for } l \neq 1 \text{ and } m \neq 1 \end{cases}. \quad (\text{E1})$$

This leads to the fact that $(D^T D)_{11}^{-1}$ is proportional to N^{-1} , while $(D^T D)_{ll}^{-1}$ ($l = 2, 3, 4, 5$) are $(Na^2)^{-1}$. Thus, we obtain the order of the precisions σ_k as

$$\sigma_k = \frac{\sigma}{\sqrt{N}} \begin{cases} O(1) & \text{for } k = 1 \\ O(1)a^{-1} & \text{for } k \neq 1 \end{cases}. \quad (\text{E2})$$

This implies that the precision of the semi-major axis does not depend on the semi-major axis itself, which is natural because the precision of the semi-major axis is equivalent to the precision of the positional determination by the astrometric measurements. We also see that the precisions of the other orbital elements are inversely proportional to the semi-major axis. In addition, it is reasonable that the precisions are inversely proportional to \sqrt{N} , because the residual of the data ϵ is assumed to be statistical errors. Since ϵ actually includes systematic errors, σ/\sqrt{N} approaches asymptotically to a value dependent on the systematic errors as N increases.

Thus, the precisions in Table F1 correspond to the values of $O(1)$ in Equation (E2), which are independent of a . In addition, these precisions are independent of the orbital element Ω , because the change of Ω corresponds to the rotation of the orbit around the line of sight, so that it never affects the shape of the orbit on the sky plane. The precisions of orbital elements are unchanged if the shape of the orbit unchanged. This independence is verified by the reduction of the integrand in Equation (D3). Therefore, σ_k ($k = 1, \dots, 5$) are uniquely determined by the orbital elements e, i , and ω , which enable us to present the expression for σ_k ($k = 1, \dots, 5$):

$$\sigma_k = \frac{\sigma}{\sqrt{N}} \begin{cases} f(e, i, \omega) & \text{for } k = 1 \\ g(e, i, \omega)a^{-1} & \text{for } k \neq 1 \end{cases}, \quad (\text{E3})$$

where

$$\begin{aligned} f &= \sqrt{N(D^T D)_{11}^{-1}} & \text{for } k = 1 \\ g &= a\sqrt{N(D^T D)_{kk}^{-1}} & \text{for } k \neq 1 \end{aligned}. \quad (\text{E4})$$

APPENDIX F: CALCULATIONAL RESULTS OF THE PRECISION FOR EACH ORBITAL ELEMENT

We show here the results obtained by calculating the precisions of orbital elements σ_k (Equation A1). We first investigate general features of the precisions. In Table F1 we show the precisions for 4 cases: $(e, i) = (0.2, 30^\circ)$, $(0.2, 60^\circ)$, $(0.8, 30^\circ)$, and $(0.8, 60^\circ)$. We adopt a constant value 0° for ω in Table F1. The units of precisions are represented as σ/\sqrt{N} for $k = 1$ and as $\sigma/a\sqrt{N}$ for $k \neq 1$. We note that the precision of the semi-major axis σ_a corresponds to $f(e, i, \omega)$ in Equation (3).

We see from Table F1 that the precision of the semi-major axis is independent of the inclination angle. This is because the change in the inclination angle does not affect the angular size of the semi-major axis when $\omega = 0^\circ$, which is the case that the semi-major axis has an overlap with the line

of intersection between the sky plane and the orbital plane. In addition, σ_a is nearly independent of the eccentricity, because the major axis is unchanged with the change of the eccentricity. Thus, when $\omega = 0^\circ$, the precision of the semi-major axis is nearly unchanged.

Table F1 also shows that the precisions of ω and Ω decrease with increase in the inclination angle. For a smaller i , which corresponds to μ close to 1, the matrix T is approximately a function of a and $\omega + \Omega$. This means that the shape of the orbit on the sky plane depends on $\omega + \Omega$, so that ω and Ω cannot be solved separately from the shape. Thus, the precisions of ω and Ω are enhanced. On the other hand, for a larger i , the shape of orbit is more dependent on both ω and Ω , so that their precisions are reduced. Here we should note that the change in the element ω has little effect on the shape of orbit in the case of a small e . Although it seems that this means a large precision of ω , the precision σ_ω appeared in Table F1 is comparable to the other precisions when $e = 0.2$ and $i = 60^\circ$. This is because difference of the velocity between different orbital phases helps ω to be determined.

In Table F2, we show the precisions when changing the argument of periapsis. We calculate the precisions for $\omega = 90^\circ$, which corresponds the situation where the major axis is perpendicular to the line of intersection between the sky plane and the orbital plane. Here we adopt $e = 0.2$ and 0.8 with a fixed i (30°). When $e = 0.2$, all precisions are nearly unchanged even if ω changes, because the shape of the orbit nearly unchanged even if ω changes when the orbit is nearly circular. On the other hand, when $e = 0.8$, Table F2 shows that the precision of the semi-major axis is clearly larger than that when $\omega = 0^\circ$. This is because the changes in a and in i have a similar effect on the shape of orbit, so that it is difficult to determine a and i separately. Thus, the precision of the semi-major axis is relatively large in the case of the large eccentricity and the argument of periapsis near 90° .

The precision of the semi-major axis depends on the inclination angle when the eccentricity is large and the argument of periapsis is close to 90° . In Table F3, we show the dependence of σ_a on i and ω when $e = 0.8$. When $\omega = 0$, σ_a do not depend on the value of i even the eccentricity is large and show the value of 1.7, which is consistent with the third and fourth lines in Table F1. On the other hand, σ_a depends on i when ω is large, and the range of σ_a increases as ω is close to 90° , which are shown in the second and third lines in Table F3. This is due to the size of the orbit. When the eccentricity is large and ω is close to 90° , the shape of the orbit on the celestial sphere significantly changes as the inclination angle changes. The orbit shows ellipse with large eccentricity when $i \sim 0$, whereas the shape of orbit appears to approach a circle with smaller semi-major axis than the original ellipse as i becomes large. If the apparent size of orbit becomes smaller, it becomes harder to measure the orbital elements by astrometry. This leads to the fact that σ_a increases as the inclination angle increases, which is more significant for ω closer to 90° . Therefore, σ_a show the large dependence on the inclination angle when the eccentricity is large and the argument of periapsis is close to 90° .

This paper has been typeset from a $\text{\TeX}/\text{\LaTeX}$ file prepared by the author.

Table F1. Calculated precisions when $\omega = 0^\circ$. We calculate them for 4 cases in which eccentricity and inclination angle take two different values. The number in subscripts of σ are replaced with the orbital elements itself. The precision σ_a is normalised with $\frac{\sigma}{\sqrt{N}}$, and those of the other orbital elements are normalised with $\frac{\sigma}{a\sqrt{N}}$.

e	i	σ_a	σ_e	σ_μ	σ_ω	σ_Ω
0.2	30°	1.4	1.1	2.0	7.4	7.3
0.2	60°	1.4	1.1	1.6	2.1	2.0
0.8	30°	1.7	2.3	6.2	9.8	8.9
0.8	60°	1.7	2.3	4.1	3.2	1.9

Table F2. Calculated precisions when $i = 30^\circ$. The value of a is the same as Table F1. We calculate them for 4 cases in which eccentricity and argument of periapsis take two different values. The number in subscripts of σ are replaced with the orbital elements itself. The normalisation of precisions is the same as Table F1. The values in the first and third lines are the same as Table F1.

e	ω	σ_a	σ_e	σ_μ	σ_ω	σ_Ω
0.2	0°	1.4	1.1	2.0	7.4	7.3
0.2	90°	1.4	1.3	2.0	7.3	7.4
0.8	0°	1.7	2.3	6.2	9.8	8.9
0.8	90°	6.3	2.6	7.0	8.7	9.8

Table F3. Calculated precisions of the semi-major axis when $e = 0.8$. The value of a is the same as Table F1. We calculate σ_a for 3 cases in which the values of the argument of periapsis are 0° , 40° , and 80° . The values of 10° and 80° are adopted as the inclination angle for each value of the argument of periapsis. The normalisation of precisions is the same as Table F1.

e	ω	$\sigma_a (i = 10^\circ)$	$\sigma_e (i = 80^\circ)$
0.8	0°	1.7	1.7
0.8	40°	2.0	2.2
0.8	80°	5.5	20